


Polarization superposition of room-temperature polariton condensation

Yuta Moriyama^{1,2}, Takaya Inukai^{1,2}, Tsukasa Hirao¹, Yusuke Ueda¹, Shun Takahashi¹ & Kenichi Yamashita¹  [✉]

A methodology for forming a qubit state is essential for quantum applications of room temperature polaritons. While polarization degree of freedom is expected as a possible means for this purpose, the coupling of linearly polarized polariton condensed states has been still a challenging issue. In this study, we show a polarization superposition of a polariton condensed states in an all-inorganic perovskite microcavity at room temperature. We achieved the energy resonance of the two orthogonally polarized polariton modes with the same number of antinodes by exploiting the blue shift of the polariton condensed state. The polarization coupling between the condensed states results in a polarization switching in the polariton lasing emission. The orthorhombic crystal structure of the perovskite active layer and/or a slight off-axis orientation of the perovskite crystal axis from the normal direction of microcavity plane enables the interaction between the two orthogonally polarized states. These observations suggest the use of polariton polarization states as a promising room temperature quantum technology.

¹Faculty of Electrical Engineering and Electronics, Kyoto Institute of Technology, Matsugasaki, Sakyo-ku, Kyoto 606-8585, Japan. ²These authors contributed equally: Yuta Moriyama, Takaya Inukai. ✉email: yamasita@kit.ac.jp

A cavity polariton is a quasiparticle formed by the strong coupling between a photon and an exciton in an optically active microcavity^{1,2}. As this bosonic quasiparticle possesses a small effective mass inherited from the photonic nature and a nonlinearity derived from the excitonic nature, the ensemble of cavity polariton particles reaches a threshold density for the Bose-Einstein condensation at a relatively high temperature. This phenomenon is known as polariton condensation (or polariton lasing)^{3,4}. Furthermore, the room-temperature (RT) polariton condensation has also been revealed in several material systems, including widegap inorganic semiconductors^{5,6}, organic semiconductors^{7–10}, transition-metal dichalcogenides^{11,12}, and lead-halide perovskites^{13–15}. To utilize the RT polaritons for future quantum technologies, a methodology for forming a qubit state that can be readily created and manipulated should be established^{16,17}. The polarization degree of freedom is a promising candidate as a means of forming the polaritonic qubit states, analogous with the photonic quantum computing systems¹⁸. In fact, anisotropic optical features of polariton modes have been widely discussed in organic semiconductors^{19–22} and perovskites^{23,24}. The Spin Meissner effect, which arises in the presence of an external magnetic field, has also been explored as a mechanism for manipulating the circular polarization state of the polariton condensed phase^{25–27}. However, a coupling of linearly polarized polariton condensed states has not been realized yet in RT polariton systems. It is a challenging issue to develop a strategy in which an energy resonance and non-zero interaction between the two orthogonally polarized states are simultaneously obtained.

In this study, we demonstrate a polarization superposition of RT polariton condensed states. In an all-inorganic perovskite microcavity, we achieve an energy resonance at the Γ point of the two orthogonally polarized modes by exploiting the blue shift of a polariton condensed state. The orthorhombic crystal structure of the perovskite active layer and/or a slight off-axis orientation of the perovskite crystal axis from the microcavity normal enable interaction between the two polarized modes. Systematic photoluminescence (PL) results show that by a non-resonant optical pulse pumping, a polarization-hybridized condensed mode can be initialized to one of the polarization directions. As a result of the polarization hybridization of polariton condensed states, furthermore, we observed a polarization-switching phenomenon in the polariton lasing operation. A detailed analysis of emission using the Stokes parameters demonstrates that the polariton condensation state can be described as a superposition of polarization. These observations demonstrate a great promise of polariton condensed states as an RT qubit technology.

Results and discussion

Room temperature polariton in CsPbBr₃ microcavity. In order to create polarization-coupled polariton condensed states, we employ an all-inorganic lead-halide perovskite, CsPbBr₃, as the anisotropic active medium in a microcavity. This compound has been demonstrated to show a high PL quantum yield and a large exciton binding energy, leading to an RT stability of exciton. Previous studies have experimentally demonstrated the RT polariton condensation in CsPbBr₃ microcavities^{13–15}. A possibility of condensation in the polaritonic Bardeen-Cooper-Schrieffer phase has been proposed for CsPbBr₃ microcavity at high excitation densities^{23,28}.

Meanwhile, anisotropic polaritonic features also gather attention [see Fig. 1a]. Polarization anisotropy of CsPbBr₃ crystal, which shows the orthorhombic structure, breaks a rotation symmetry of the microcavity system, inducing a ‘X–Y’ polarization splitting in lower polariton branches (LPBs) at the Γ point

[see Fig. 1b]^{23,24}. The LPB splits also into transverse-electric (TE) and transverse-magnetic (TM) modes at large wavevector regions because of quasi-optical spin-orbit-coupling [see Fig. 1b]^{23,29,30}. These dispersion characteristics lead to polarization-dependent polariton lasing phenomena: Spencer et al. have reported that the split LPB modes show an independent polariton lasing at the energy position of each polarization mode²³. Li et al. have reported in a study of liquid crystal-filled CsPbBr₃ microcavity that circularly polarized polariton lasing occurs from LPB modes split in in-plane wavenumber direction by optical Rashba–Dresselhaus coupling³⁰. However, a coupling between linearly polarized condensed states has not been reported. For this purpose, we need to meet two requirements: (i) a fine-tuning of X–Y energy resonance and (ii) a non-zero interaction between the X- and Y-polarized states. The X–Y energy resonance must be arranged for the LPB modes having the same number of antinodes, and the spatial distribution of wavefunctions along the vertical direction should be the same for the two polarizations. In CsPbBr₃ microcavity, however, a fine-tuning of the X- and Y-polarized modes with the same antinode number is impossible because they are originally detuned due to the X–Y splitting. To overcome this problem, we exploit the blue shift of the polariton condensed state that emerges at the above-threshold density.

Coupling of polariton condensed modes. We show angle-resolved PL results for a CsPbBr₃ microcavity fabricated with a solution-based crystallization method^{28,31–34}. Figures S1–S3 in the Supplementary Information depict the fabrication procedure, microscopic images of fabricated crystals, and optical properties of the microcavity, respectively. The quality factor is evaluated from transmission measurement to be ~ 180 . A schematic diagram of the Fourier-space imaging setup is shown in Fig. S4 in the Supplementary Information. One can find details of the experimental methods in the Method section. In the angle-resolved PL measurements, X- and Y-polarizations correspond to TE and TM polarizations, respectively [see Fig. 1c]. Figure 1d shows colormaps of linearly polarized angle-resolved PL results obtained under the various pumping fluence P . The full dataset is shown in Fig. S5 in the Supplementary Information. At P as low as $\sim 245 \mu\text{J}/\text{cm}^2$, we find that the LPB modes at both polarizations are in the strong coupling regime and show a parabolic dependence on the in-plane wavevector k_y around zero [see panels (i) and (v) of Fig. 1d]. Rabi splitting energies are evaluated from the fitting analyses using a coupled oscillator model to be 62 meV and 45 meV for the X-polarized and Y-polarized LPB modes, respectively (see Supplementary Text S1 and Fig. S6 in the Supplementary Information). The X–Y splitting energy at $k_y \sim 0$ is ~ 6.1 meV at the lowest P in this measurement. The mode number for both the X- and Y-polarized modes is three, which is expected from the group index (~ 2.4) and the crystal thickness (~ 440 nm). In this measurement, the quality factor Q was found to be not very large ($Q \sim 200$), which may be due to unexpected losses in the cavity and can be improved in future studies.

In the X-polarization, the parabolic LPB mode disappears at $P \sim 449 \mu\text{J}/\text{cm}^2$, and instead, a highly directional PL signal appears at ~ 2.316 eV [see panel (ii) of Fig. 1d]. Furthermore, the emission intensity that reflects the polariton density shows a threshold behavior [see Fig. 1e], indicating the RT condensation of polariton particles. With increasing P , the energy of the condensed state shows a blue shift [see panel (iii) of Fig. 1d] caused by polariton–polariton interaction. It should be noted that the energy of the blue-shifted condensed state is ~ 2.330 eV, which already exceeds the energy of Y-polarized LPB mode at $k_y \sim 0$ [~ 2.322 eV, see panel (v) of Fig. 1d].

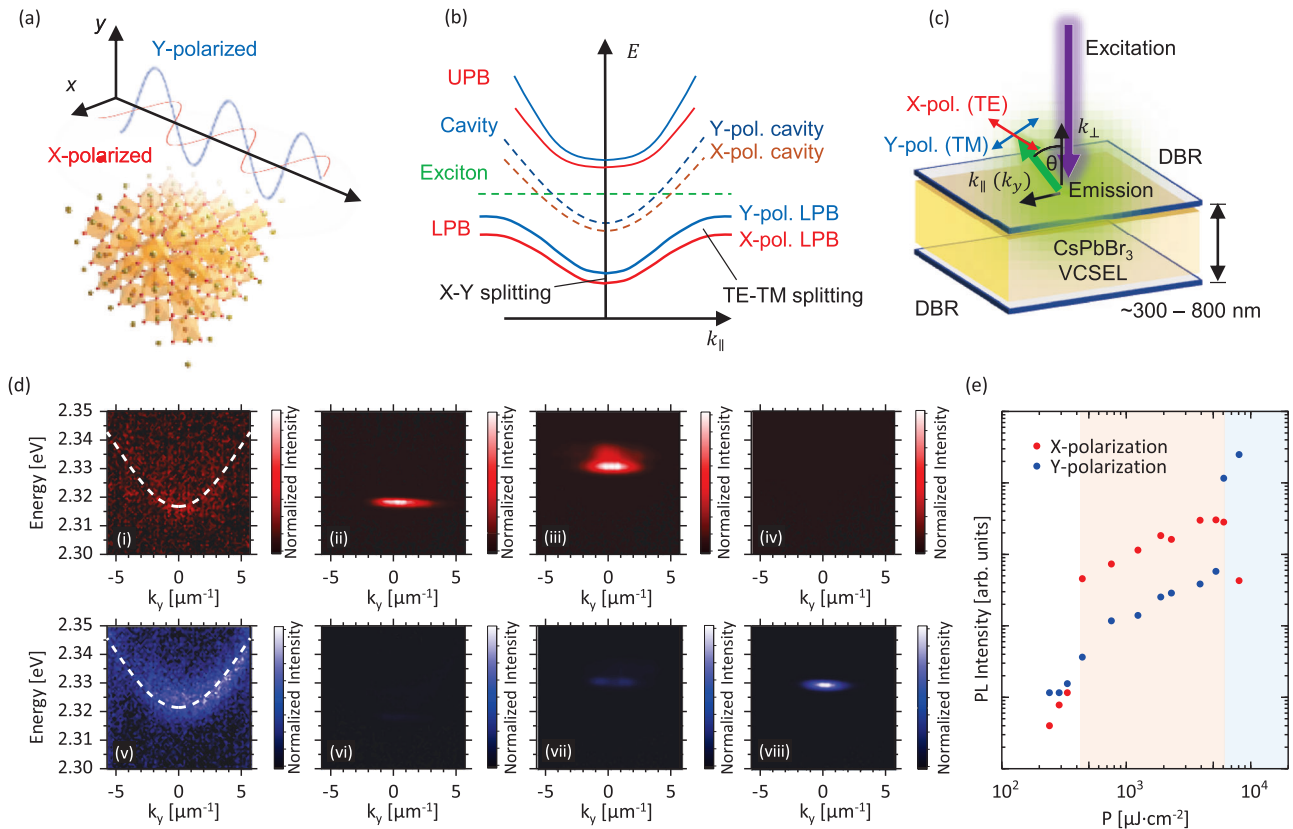


Fig. 1 CsPbBr₃ microcavity with X–Y splitting. **a** A schematic of a CsPbBr₃ crystal and electromagnetic waves with orthogonal polarizations. **b** A schematic of dispersion curves with X–Y splitting and TE–TM splitting in LPB and UPB modes. **c** A schematic showing the configuration of angular-dependent PL measurement. **d** Colormaps of X-polarized [panels (i–iv)] and Y-polarized [panels (v–viii)] angle-resolved PL. Pumping fluences P are (i, v) 245, (ii, vi) 449, (iii, vii) 1260, and (iv, viii) 8170 $\mu\text{J}/\text{cm}^2$. **e** P -dependence of PL signal intensity at the Γ point. Red and blue circles plot the data at X- and Y-polarizations, respectively.

A further increase in P ($>\sim 6150 \mu\text{J}/\text{cm}^2$) leads to the second threshold behavior for the Y-polarized LPB mode [see panel (viii) of Fig. 1d]. Interestingly, we find a drastic switching in the PL signal intensities between the two polarized states at the second threshold, where the Y-condensed state almost disappears [see panel (iv) of Fig. 1d], i.e. polarization switching. To the best of our knowledge, this phenomenon is observed for the first time in this study and is clearly different from a previous observation showing independent polariton lasing from orthogonally polarized LPB modes²³.

To track detailed footprints of the X- and Y-polarized states, we exhibit P -dependent PL spectra at $k_x = k_y \sim 0$ [see Fig. 2a]. We divide the experimental results into three pumping fluence ranges; namely, the first range is below the first threshold ($P < \sim 340 \mu\text{J}/\text{cm}^2$), the second range is between the first threshold and the second threshold, and the third one is above the second threshold ($P > \sim 5330 \mu\text{J}/\text{cm}^2$). In the range below the first threshold, the X–Y split two LPB modes are independently observed. This is seen as two polarization degree (PD) signals with opposite signs, as shown in panels (i)–(iii) of Fig. 2b. Here, the PD is defined as

$$PD = \frac{I_X - I_Y}{I_X + I_Y}, \quad (1)$$

where I_X and I_Y are PL intensities at the X- and Y-polarizations, respectively, and is identical to the Stokes parameter S_1 described later. The X-polarized signal shows an onset of condensation at P just before the threshold.

In the second range, a PL signal showing the polariton condensation is observed at ~ 2.320 eV in the X polarization [see panel (iv) of Fig. 2b]. In addition to the conventional blue shift with the increased P , we find that the condensed mode is not perfectly polarized to the X direction but exhibits a small Y-polarized component. This fact is clearly found in normalized PL colormaps shown in Fig. S7 in the Supplementary information. More importantly, the blue-shifted condensed state exhibits an “energy hopping” from ~ 2.32 to ~ 2.33 eV at $P \sim 1260 \mu\text{J}/\text{cm}^2$ [see panels (v) and (vi) in Fig. 2b]. These results suggest the emergence of X–Y polarization coupling in the polariton condensed states. The coupling is made possible by the energetic resonance between the blue-shifted X-polarized condensed state and the Y-polarized LPB mode. It is worth noting that the coupling can be established even though the Y-polarized mode may still be incoherent. Meanwhile, non-zero interaction between the two modes is achieved by the orthorhombic crystal structure of CsPbBr₃, which will be discussed later in detail, leading to the polarization hybridization of polariton condensed state. Note that our results do not show independent condensations of the X- and Y-polarized LPB modes because the energy of the two orthogonally polarized PL are the same within this pumping fluence range.

In the third pumping fluence range ($P > \sim 6150 \mu\text{J}/\text{cm}^2$), the X-polarized condensed state shifts to ~ 2.34 eV and is completely separated from the energy of the Y-polarized state [see panels (xi) and (xii) of Fig. 2b]. Meanwhile, the polarization of the condensed state at ~ 2.33 eV switches to Y-polarization, leading to polarization switching.

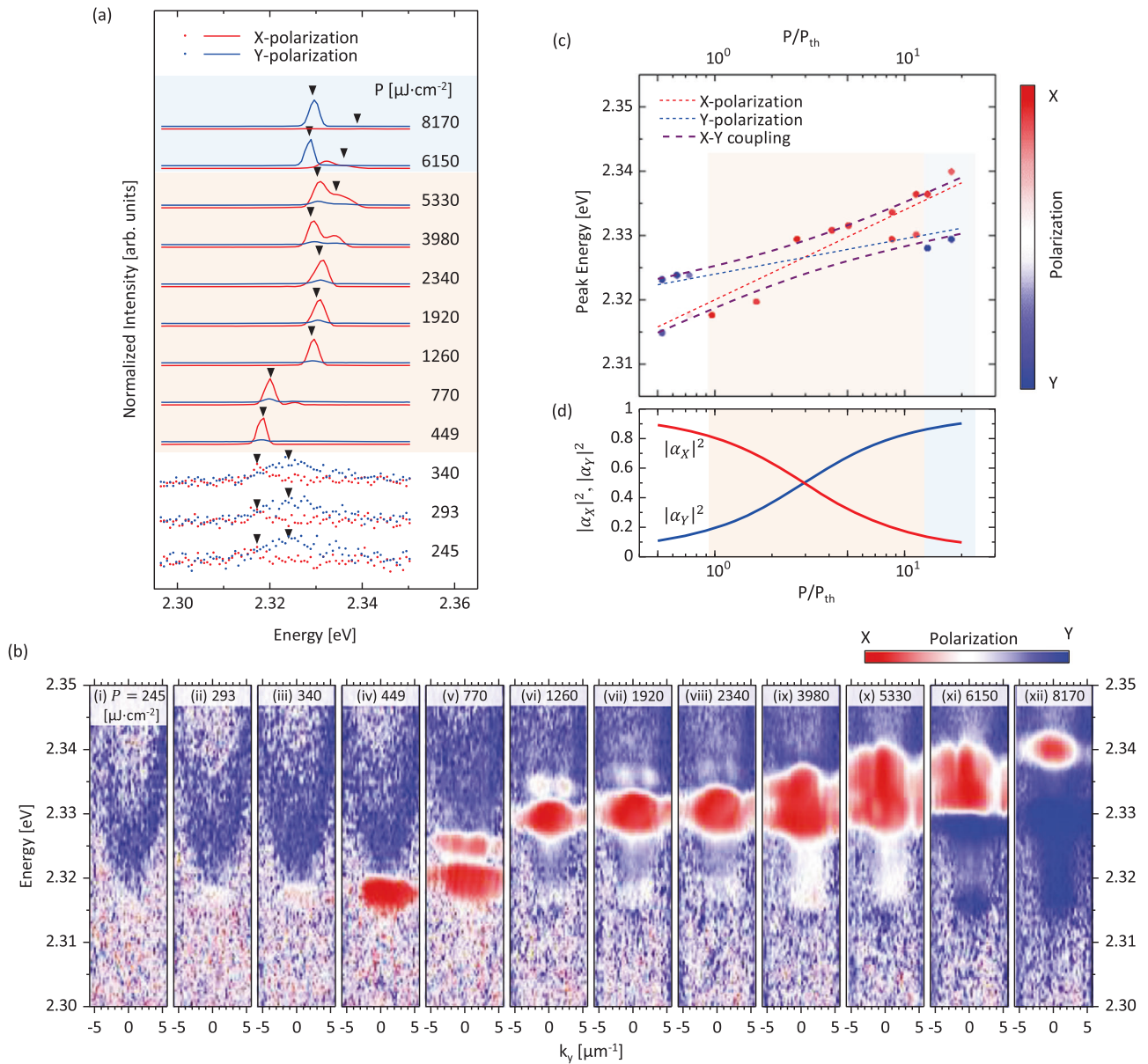


Fig. 2 Polarization coupling of polariton condensed state in CsPbBr₃ microcavity. **a** P -dependent PL spectra at the Γ point. Red and blue curves show X- and Y-polarization, respectively. Orange and blue shaded region show the second and third ranges of P , which describe in the main text. No shaded region indicates the first range of P . **b** Colormaps of polarization degrees for polariton signals recorded at various P . **c** Peak energies of PL signals as functions of P . Colors of each plot show the polarization degree of the signals. Dashed lines exhibit functions derived from a fitting analysis using Eqs. (2) and (3). **d** $|\alpha_X|^2$ and $|\alpha_Y|^2$ for polarization coupled LPB mode calculated from the fitting results. This result exhibits one of the results for the lower mode. For the higher mode, curves for $|\alpha_X|^2$ and $|\alpha_Y|^2$ are simply exchanged.

We employ a simple model to formulate our results. The coupling between the X- and Y-polarized states is described well by a coupling model with a phenomenological Hamiltonian of

$$\begin{bmatrix} E_X & V \\ V & E_Y \end{bmatrix} \begin{bmatrix} \alpha_X \\ \alpha_Y \end{bmatrix} = E_c \begin{bmatrix} \alpha_X \\ \alpha_Y \end{bmatrix}. \quad (2)$$

Here, E_X and E_Y are energies of uncoupled X- and Y-polarized states, and E_c is the eigenenergy of X-Y coupled state. We assume that the interaction term V is constant against the polariton density. $|\alpha_X|^2$ and $|\alpha_Y|^2$ show the fractions of X- and Y-polarized states, respectively. In Gross-Pitaevskii equation, the blue shift of E_X or E_Y (ΔE) is described to be proportional to the density of polariton particles, N_{pol} ^{1,35–37}. On the other hand, previous reports have shown that the experimentally observed ΔE follows a

logarithmic function on P ^{38,39}. We employ the latter case and express ΔE as a logarithmic function on P .

$$\Delta E(P/P_{th}) = C \log(P/P_{th} - 1) \quad (3)$$

Here, C is a constant and P/P_{th} is the pumping fluence normalized by that at the threshold.

Figure 2c compares the experimental result and the theoretical model shown above, revealing that the model can express the experimental result well. V is estimated to be ~ 2.6 meV. In Fig. 2d, we find that the two polarized states are hybridized well when $|\alpha_X|^2$ and $|\alpha_Y|^2$ are in a range of 0.2–0.8, which approximately corresponds to the second range on P . Interestingly, the condensed mode in this range is successfully “initialized” to the X polarization by the non-resonant pulse

pumping. When $|\alpha_X|^2$ and $|\alpha_Y|^2$ are outside this range, the hybridization becomes small, and thus the independent polariton condensation appear in the third range of P .

It should be noted that the doublet of cross-polarized components is not clearly observed in the second range on P . While we have not identified the cause of this phenomenon within the scope of this study, one potential contributing factor may be that our experiments rely on emission signals to determine the energy levels of modes, which is proportional to the population of excited particles (i.e., polariton particles). Consequently, states with short lifetimes are challenging to observe, similar to the general difficulty in observing emission from upper polariton branches. The relaxation dynamics, based on polariton lifetimes at each energy level, warrant detailed investigation and present an intriguing avenue for future research. Nevertheless, from the viewpoint of application as a quantum technology, this is an interesting finding indicating that the polariton condensed states formed by the optical pumping are initialized to one of the polarization states.

Here, we discuss the origins of interaction between the X- and Y-polarizations. As shown in a recent paper⁴⁰, the mode coupling equation at an energetic resonant condition between the orthogonally polarized cavity photon modes with the same number of antinodes is expressed as

$$E \begin{bmatrix} \alpha_X \\ \alpha_Y \end{bmatrix} = \left\{ \begin{bmatrix} E_X & 0 \\ 0 & E_Y \end{bmatrix} + \frac{(\hbar c)^2}{\varepsilon_{zz}} \begin{bmatrix} \varepsilon_{xx}k_x^2 + \tilde{\varepsilon}_{zz}k_y^2 & (\varepsilon_{yy} - \varepsilon_{zz})k_yk_x \\ (\varepsilon_{xx} - \tilde{\varepsilon}_{zz})k_yk_x & \varepsilon_{zz}k_x^2 + \varepsilon_{yy}k_y^2 \end{bmatrix} \right\} \begin{bmatrix} \alpha_X \\ \alpha_Y \end{bmatrix}. \quad (4)$$

Here ε_{ij} denotes the dielectric tensor inside the cavity, and $\tilde{\varepsilon}_{zz} = \varepsilon_{zz} + \varepsilon_{xz}\varepsilon_{zx}/\varepsilon_{zz}$. Note that Eq. (4) is equivalent to Eq. (2), and we focus on the non-diagonal terms here. For CsPbBr₃ showing the orthorhombic crystal structure at RT, we thus obtain $\varepsilon_{xx} \neq \varepsilon_{yy} \neq \varepsilon_{zz}$ under the assumption that one of the crystal axes is along the normal direction of the microcavity surface. Furthermore, as the wavefunction of polariton condensed state is localized in the real space and shows a spread in the wavenumber space, we take into account not only the origin of wavenumber space but also the vicinity of it. We should note two things, that are (i) the function of k_yk_x is not always an odd function but behaves as an even function when the coordinates are rotated by 45° around the energy axis (see Fig. S8 in the Supplementary Information) and (ii) in general, the wavefunction of polariton condensate state is not symmetrically spread in the radial direction²⁴. As a consequence, we should consider that k_yk_x is not perfectly zero, and thus the off-diagonal terms, $(\varepsilon_{xx} - \tilde{\varepsilon}_{zz})k_yk_x$ and $(\varepsilon_{yy} - \varepsilon_{zz})k_yk_x$, are found to be non-zero in a CsPbBr₃ microcavity, showing that the polarization coupling is possible. Note that the off-diagonal terms become zero in the case of highly symmetric crystal (i.e. $\varepsilon_{xx} = \varepsilon_{yy} = \varepsilon_{zz}$) or in the case of too strong anisotropy (too large detuning between the X- and Y- modes). From these aspects, it is noteworthy that the CsPbBr₃ microcavity can fulfill these two requirements simultaneously owing to the ‘very small’ anisotropy. We know that the non-zero off-diagonal terms discussed here might be small values, but in a cavity with high quality factor, the overall hybridization degree is significantly enhanced in an optical cavity.

In addition to the non-zero off-diagonal terms discussed above, we might consider the deviation of the CsPbBr₃ crystal axis from the normal direction to the microcavity as another unexpected reason for the X–Y polarization coupling. As shown in Fig. S9 in the Supplementary Information, we occasionally observe LPB modes with the X–Y splitting showing non-clean polarization features. As such, the misalignment leads to the nonzero off-

diagonal terms, and crystal growth techniques, in which the crystal orientation can be strictly controlled, are highly required.

Evaluation of polarization states. Finally, we validate the polarization state of the coupled polariton condensed states. We show the angle-resolved PL results for the complete polarization components, encompassing the horizontal/vertical (i.e., I_X/I_Y), diagonal/anti-diagonal (I_D/I_A), and right-circular/left-circular (I_R/I_L) polarizations in the vicinity of the first threshold (Fig. S10 in the Supplementary Information). This measurement was performed for a shifted position within the same crystal, resulting in a slightly elevated energy level of the LPB states compared to the results mentioned above. Below the threshold, there is no significant difference in the polarization components of PL intensities. Stokes parameters, denoted as $S_1 = (I_X - I_Y)/(I_X + I_Y)$, $S_2 = (I_D - I_A)/(I_D + I_A)$, and $S_3 = (I_R - I_L)/(I_R + I_L)$, approximate zero values, indicating that the polarization state below the threshold resides in a ‘mixed state’. Around the threshold, as shown in Fig. 3a, I_X markedly increases to 0.5 or higher due to the onset of polariton condensation, resulting in a positive value for S_1 [see Fig. 3c]. Importantly, I_A also increases concurrently with I_X , whereas I_D remains relatively weak. In Fig. 3d, the parameter $S_0 (= \sqrt{S_1^2 + S_2^2 + S_3^2})$, which characterizes the degree of polarization, substantially rises to 0.8 above or at the threshold fluence. This high degree of polarization persists up to at least $\sim 1.6 P_{th}$, demonstrating that the polariton condensed state approaches a ‘pure polarization state’ undergoing the polarization superposition. On the other hand, S_3 remains close to zero, even beyond the threshold. This observation is consistent with the X–Y coupling described by Eq. (4), which exhibits mixing with off-diagonal terms of real numbers, resulting in the conversion to the diagonal and/or anti-diagonal polarization modes. Nevertheless, it is noteworthy that S_2 undergoes significant variations, including a change in sign [see Fig. 3b, c], suggesting the potential for quantum manipulation of the polarization state in the polariton condensed state. Further refinement of pumping fluence and exploration of synergies with the Rashba-Dresselhaus coupling effect is expected to facilitate comprehensive manipulation of the polarization state on the Poincaré sphere.

Conclusions

We demonstrated a polarization superposition of RT polariton condensed states. CsPbBr₃ crystal, which has proven to be an excellent medium for the RT polariton condensation, exhibits an anisotropic feature suitable for achieving the polarization superposition. Specifically, the orthorhombic crystal structure of CsPbBr₃ can simultaneously address the two requirements: small but non-zero X–Y splitting and non-zero off-diagonal interaction terms. By exploiting the blue shift of the polariton condensed state, we tuned energies of two orthogonally polarized modes, leading to the polarization superposition of the RT polariton condensed state.

The results shown here imply a great promise of polariton as RT quantum technologies. The polarization superposition is considerable progress toward the RT polariton qubit and quantum simulator. As a future work, it is intriguing to challenge the demonstrations of interactions between the polariton qubits and operations as a quantum logic gate. These challenges would open new perspectives on quantum applications of polaritons.

Methods

Microcavity fabrication. Distributed Bragg reflectors (DBRs) used in this study were multilayers of SiO₂ and TiO₂ on BK7 glass plates (area: 10 × 10 mm² and thickness 0.5 mm). The rf-magnetron sputtering method was employed for the deposition of nine pairs of

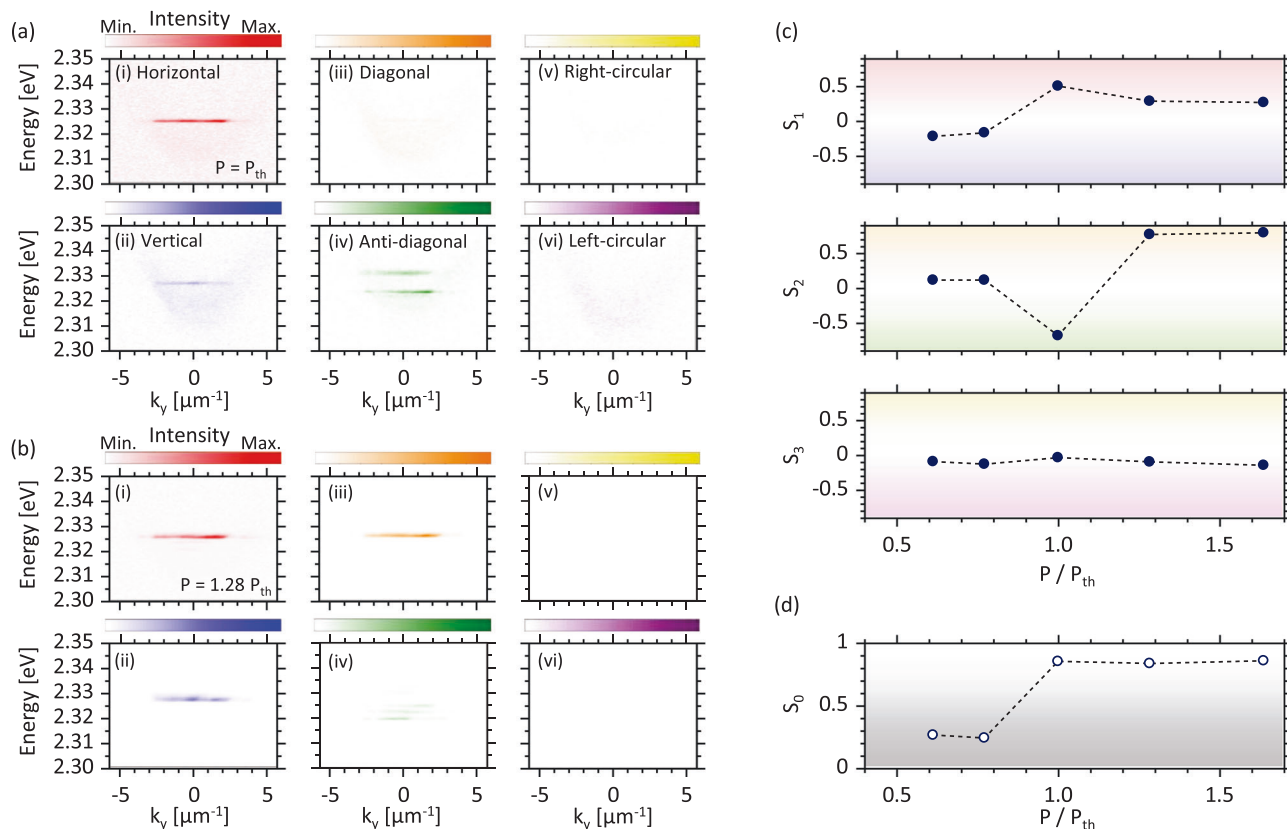


Fig. 3 Polarization states of polariton condensed states in CsPbBr₃ microcavity. **a, b** Colourmaps of angle-resolved PL spectra observed at pumping fluences of $-P_{th}$ (**a**) and $-1.28P_{th}$ (**b**). PL intensities at horizontal, vertical, diagonal, anti-diagonal, right-circular, and left-circular polarizations are shown in panels (i)–(vi), respectively. The intensities are normalized in each pumping fluence. **c** Pumping fluence dependencies of Stokes parameters, S_1 , S_2 , and S_3 . **d** Pumping fluence dependencies of Stokes parameter S_0 .

SiO₂ and TiO₂ layers. In this study, we used two types of DBRs. One of them had a reflection band (>98%) of ~450–550 nm and was used as the top mirror. The other had a reflection band of ~500–600 nm and was used as the bottom mirror.

To prepare precursor solutions of CsPbBr₃ perovskite, cesium bromide (CsBr) and lead(II) bromide (PbBr₂) were purchased from TCI. Dimethyl sulfoxide (DMSO) was purchased from Nacalai Tesque. We dissolve CsBr and PbBr₂ in DMSO in a molar ratio of 1:1 at a concentration of 0.5 M, stirred at 700 rpm with a screw tube and a stirring bar for ~1 h at 50 °C.

CsPbBr₃ microcavities were fabricated by a solution-processed crystallization method, as shown in Fig. S1 in the Supplementary Information. First, the two DBR mirrors mentioned above were washed with ultrasonic cleaning in ethanol and acetone for 10 min each and with UV ozone for 15 min. We cast the 10 μl of supersaturated precursor solution on a bottom DBR mirror. After that, the sample was capped with a top DBR mirror and then pinched with a double clip (19 mm). The crystal was grown at room temperature for one day. Next, we injected 1 μl of precursor solution into the gap of DBR mirrors using a micropipette from the three sides of the sample. The crystal was then grown further for one day at room temperature. This procedure was repeated for 4–5 times without intervals. Finally, we injected a pure solvent into the gap and dissolved all crystals once. The sample was left in atmospheric condition for 3–4 days at 50 °C to re-grow a large-sized crystal again. After the growth, we removed the DMSO solvent using ethanol. Three days later, we removed the double clip. The thickness of the crystal depended on the strength of the clipping and the amount of solution at the casting stage and was typically in a range of 300–700 nm.

Characterizations. All optical measurements were performed in atmospheric conditions (~23 °C and ~40 %RH). We used a pulse laser (FTSS355-Q4, CryLas) for sample excitation. The emission spectra were measured with a CCD spectrometer (Kymera 328i & Newton DU971PBV, Oxford ANDOR). The emission counts were recorded with a time-integration of 1 s and an accumulation of 10 times. In angle-resolved PL measurements, we used a Fourier space imaging setup (see Fig. S4 in the Supplementary Information) using an objective with NA ~ 0.5 (UPLFLN 20X, Olympus). The angle limits of angle-resolved measurement are estimated from a relationship of $\theta_{max} = \sin^{-1}(NA)$ to be 30°. Polarization measurements were performed by using a Glan–Thompson prism as the polarizer and a quartz quarter-wave plate. Spectral resolution of the measurement system was up to ~0.4 nm.

Data availability

The datasets generated during and/or analyzed during the current study are available from the corresponding author upon reasonable request.

Received: 27 November 2023; Accepted: 7 December 2023;
Published online: 20 December 2023

References

1. Kavokin, A. V. et al. *Microcavities*. (Oxford University Press, 2017).
2. Weisbuch, C., Nishioka, M., Ishikawa, A. & Arakawa, Y. Observation of the coupled exciton-photon mode splitting in a semiconductor quantum microcavity. *Phys. Rev. Lett.* **69**, 3314–3317 (1992).

3. Kasprzak, J. et al. Bose–Einstein condensation of exciton polaritons. *Nature* **443**, 409–414 (2006).
4. Deng, H., Weihs, G., Santori, C., Bloch, J. & Yamamoto, Y. Condensation of semiconductor microcavity exciton polaritons. *Science* **298**, 199–202 (2002).
5. Christopoulos, S. et al. Room-temperature polariton lasing in semiconductor microcavities. *Phys. Rev. Lett.* **98**, 126405 (2007).
6. Lai, Y.-Y., Lan, Y.-P. & Lu, T.-C. Strong light–matter interaction in ZnO microcavities. *Light Sci. Appl.* **2**, e76–e76 (2013).
7. Kéna-Cohen, S. & Forrest, S. R. Room-temperature polariton lasing in an organic single-crystal microcavity. *Nat. Photon* **4**, 371–375 (2010).
8. Daskalakis, K. S., Maier, S. A., Murray, R. & Kéna-Cohen, S. Nonlinear interactions in an organic polariton condensate. *Nat. Mater.* **13**, 271–278 (2014).
9. Plumhof, J. D., Stöferle, T., Mai, L., Scherf, U. & Mahrt, R. F. Room-temperature Bose–Einstein condensation of cavity exciton–polaritons in a polymer. *Nat. Mater.* **13**, 247–252 (2014).
10. Yamashita, K. et al. Ultrafast dynamics of polariton cooling and renormalization in an organic single-crystal microcavity under nonresonant pumping. *ACS Photonics* **5**, 2182–2188 (2018).
11. Zhao, J. et al. Ultralow threshold polariton condensate in a monolayer semiconductor microcavity at room temperature. *Nano Lett.* **21**, 3331–3339 (2021).
12. Anton-Solanas, C. et al. Bosonic condensation of exciton–polaritons in an atomically thin crystal. *Nat. Mater.* **20**, 1233–1239 (2021).
13. Su, R. et al. Room-temperature polariton lasing in all-inorganic perovskite nanoplatelets. *Nano Lett.* **17**, 3982–3988 (2017).
14. Su, R. et al. Room temperature long-range coherent exciton polariton condensate flow in lead halide perovskites. *Sci. Adv.* **4**, eaau0244 (2018).
15. Bao, W. et al. Observation of Rydberg exciton polaritons and their condensate in a perovskite cavity. *Proc. Natl Acad. Sci. USA* **116**, 20274–20279 (2019).
16. Ghosh, S. & Liew, T. C. H. Quantum computing with exciton-polariton condensates. *npj Quantum Inf.* **6**, 16 (2020).
17. Kavokin, A. et al. Polariton condensates for classical and quantum computing. *Nat. Rev. Phys.* <https://doi.org/10.1038/s42254-022-00447-1> (2022).
18. Slussarenko, S. & Pryde, G. J. Photonic quantum information processing: a concise review. *Appl. Phys. Rev.* **6**, 041303 (2019).
19. Litinskaya, M., Reineker, P. & Agranovich, V. M. Exciton-polaritons in a crystalline anisotropic organic microcavity. *Phys. Stat. Sol. A* **201**, 646–654 (2004).
20. Zoubi, H. & La Rocca, G. Microscopic theory of anisotropic organic cavity exciton polaritons. *Phys. Rev. B* **71**, 235316 (2005).
21. Kéna-Cohen, S., Davanço, M. & Forrest, S. R. Strong exciton-photon coupling in an organic single crystal microcavity. *Phys. Rev. Lett.* **101**, 116401 (2008).
22. Tagami, T. et al. Anisotropic light-matter coupling and below-threshold excitation dynamics in an organic crystal microcavity. *Opt. Express* **29**, 26433–26443 (2021).
23. Spencer, M. S. et al. Spin-orbit-coupled exciton-polariton condensates in lead halide perovskites. *Sci. Adv.* **7**, eabj7667 (2021).
24. Li, H. et al. Localization of anisotropic exciton polariton condensates in perovskite microcavities. *Appl. Phys. Lett.* **120**, 011104 (2022).
25. Larionov, A. V. et al. Polarized nonequilibrium Bose-Einstein condensates of spinor exciton polaritons in a magnetic field. *Phys. Rev. Lett.* **105**, 256401 (2010).
26. Walker, P. et al. Suppression of Zeeman splitting of the energy levels of exciton-polariton condensates in semiconductor microcavities in an external magnetic field. *Phys. Rev. Lett.* **106**, 257401 (2011).
27. Król, M. et al. Giant spin Meissner effect in a nonequilibrium exciton-polariton gas. *Phys. Rev. B* **99**, 115318 (2019).
28. Enomoto, S. et al. Drastic transitions of excited state and coupling regime in all-inorganic perovskite microcavities characterized by exciton/plasmon hybrid natures. *Light Sci. Appl.* **11**, 8 (2022).
29. Tao, R. et al. Halide perovskites enable polaritonic XY spin Hamiltonian at room temperature. *Nat. Mater.* **21**, 761–766 (2022).
30. Li, Y. et al. Manipulating polariton condensates by Rashba-Dresselhaus coupling at room temperature. *Nat. Commun.* **13**, 3785 (2022).
31. Nguyen, V.-C., Katsuki, H., Sasaki, F. & Yanagi, H. Optically pumped lasing in single crystals of organometal halide perovskites prepared by cast-capping method. *Appl. Phys. Lett.* **108**, 261105 (2016).
32. Chen, Z. et al. Thin single crystal perovskite solar cells to harvest below-bandgap light absorption. *Nat. Commun.* **8**, 1890 (2017).
33. Wang, X., Li, W., Liao, J. & Kuang, D. Recent advances in halide perovskite single-crystal thin films: fabrication methods and optoelectronic applications. *Sol. RRL* **3**, 1800294 (2019).
34. Fujiwara, K. et al. Excitation dynamics in layered lead halide perovskite crystal slabs and microcavities. *ACS Photonics* **7**, 845–852 (2020).
35. Deng, H., Haug, H. & Yamamoto, Y. Exciton-polariton Bose-Einstein condensation. *Rev. Mod. Phys.* **82**, 1489–1537 (2010).
36. Sanvitto, D. & Kéna-Cohen, S. The road towards polaritonic devices. *Nat. Mater.* **15**, 1061–1073 (2016).
37. Yagafarov, T. et al. Mechanisms of blueshifts in organic polariton condensates. *Commun. Phys.* **3**, 18 (2020).
38. Thunert, M. et al. Cavity polariton condensate in a disordered environment. *Phys. Rev. B* **93**, 064203 (2016).
39. Su, R. et al. Observation of exciton polariton condensation in a perovskite lattice at room temperature. *Nat. Phys.* **16**, 301–306 (2020).
40. Rechcińska, K. et al. Engineering spin-orbit synthetic Hamiltonians in liquid-crystal optical cavities. *Science* **366**, 727–730 (2019).

Acknowledgements

K.Y. acknowledges funding from Japan Society for the Promotion of Science, JSPS KAKENHI (Nos. 20KK0088, 22K18794, and 22H00215), and from JST CREST (JPMJCR02T4).

Author contributions

Y.M. and K.Y. conceived and planned the experiments. Y.M., T.I., and Y.U. performed the optimization of crystal growth and device fabrication. Y.M., T.I., and T.H. performed the construction of a Fourier-space imaging setup and optical measurements. Y.M., S.T., and K.Y. deeply discussed the experimental results. Y.M. and K.Y. drafted the manuscript and compiled figures, with a discussion of results and feedback from all authors.

Competing interests

The authors declare no competing interests.

Additional information

Supplementary information The online version contains supplementary material available at <https://doi.org/10.1038/s43246-023-00440-w>.

Correspondence and requests for materials should be addressed to Kenichi Yamashita.

Peer review information *Communications Materials* thanks the anonymous reviewers for their contribution to the peer review of this work. Primary Handling Editor: Aldo Isidori.

Reprints and permission information is available at <http://www.nature.com/reprints>

Publisher's note Springer Nature remains neutral with regard to jurisdictional claims in published maps and institutional affiliations.



Open Access This article is licensed under a Creative Commons Attribution 4.0 International License, which permits use, sharing, adaptation, distribution and reproduction in any medium or format, as long as you give appropriate credit to the original author(s) and the source, provide a link to the Creative Commons license, and indicate if changes were made. The images or other third party material in this article are included in the article's Creative Commons license, unless indicated otherwise in a credit line to the material. If material is not included in the article's Creative Commons license and your intended use is not permitted by statutory regulation or exceeds the permitted use, you will need to obtain permission directly from the copyright holder. To view a copy of this license, visit <http://creativecommons.org/licenses/by/4.0/>.

© The Author(s) 2023